

# Deep-Blue Thermally Activated Delayed Fluorescence Emitters Containing Diphenyl Sulfone Group for Organic Light Emitting Diodes

In Hye Lee<sup>1</sup>, Ki Ju Kim<sup>1</sup>, Young Kwan Kim<sup>2,\*</sup>, Young Sik Kim<sup>2,\*</sup>, and Dong Myung Shin<sup>1,\*</sup>

<sup>1</sup>Department of Chemical Engineering, Hongik University, Seoul 04066, Korea

<sup>2</sup>Department of Information Display, Hongik University, Seoul 04066, Korea

Novel blue thermally activated delayed fluorescence (TADF) emitters, **D1-DPS** and **D2-DPS**, were designed and synthesized. Diphenyl sulfone (DPS) group functioned as a common acceptor, and it combined with each of two different spiro-acridine groups, D1 and D2. The calculated energy differences ( $\Delta E_{ST}$ ) of the singlet and triplet excited states of **D1-DPS** (0.062 eV) and **D2-DPS** (0.128 eV) had sufficiently small  $\Delta E_{ST}$  values, which is favorable in the thermally activated reverse intersystem crossing (RISC) process from the  $T_1$  state to the  $S_1$  state. A device doped 10 wt% of **D2-DPS** with ADN host material, obtained 5.05% of external quantum efficiency with deep-blue emission having CIE<sub>xy</sub> coordinates of (0.152, 0.065). The results showed that these molecules are promising host-free TADF deep-blue emitters by inhibiting concentration quenching.

**Keywords:** Organic Light Emitting Diodes, Thermally Activated Delayed Fluorescence, Deep-Blue Emitter, Diphenyl Sulfone Derivative.

## 1. INTRODUCTION

Organic light emitting diodes (OLED) are an attractive technology because they can be used in a variety of sizes and shapes, high-resolution flat panel displays, and power consumption.<sup>1-4,6,13</sup> The internal quantum efficiency ( $\eta_{int}$ ), which is the quantum statistical branching ratio of the electron-hole pairs under electrical excitation, is limited to 25% because of the forbidden spin of the radiative decay of triplet excitons. However, phosphorescent OLEDs (PHOLEDs) can obtain an  $\eta_{int}$  of 100%.<sup>2,4,6</sup> To overcome the disadvantages of PHOLEDs, such as lower electroluminescence (EL) efficiency under high current density, and low reliability in the blue region of the visible spectrum, a new concept of thermally activated delayed fluorescence (TADF) was considered in several works published.<sup>2,4,6</sup>

The third generation of OLED materials, TADF materials have attracted much interest because of their stability, high efficiency, and flexible molecular structure.<sup>1-4</sup> TADF molecules have shown the thermally activated up-conversion of non-emissive triplet ( $T_1$ ) excitons to emissive singlet ( $S_1$ ) excitons through an intersystem crossing

(ISC) by using sufficiently small energy difference ( $\Delta E_{ST}$ ) between the lowest singlet ( $S_1$ ) and lowest triplet ( $T_1$ ) excited states.<sup>4</sup> This capability can achieve high external EL quantum efficiencies ( $\eta_{ext}$ ), and realize 100% of  $\eta_{int}$  when the rate of ISC from  $T_1$  into  $S_1$  is much higher than the competing rate of the non-radiative decay for  $T_1$ .<sup>4-5</sup> This property can be controlled by the optimization of the chemical structural feature and the detailed understanding of the structure-property relationship.<sup>1,5</sup> Recently, versatile TADF molecular systems were reported, including spiro-acridine,<sup>6</sup> spirobifluorene, and diphenyl sulfone (DPS) derivatives.<sup>1,6</sup> A blue TADF material (DMAC-DPS) containing DPS group showed an external quantum efficiency of 19.5% with an emission peak at 450 nm<sup>2</sup>. However, this material requires enhancement to solve the problem of lower maximum brightness and efficiency roll-off at high brightness.<sup>5</sup>

In this paper, we describe the structural calculation and synthesis as well as the photo-phycochemical characteristics of two deep-blue emitter materials, which are types of donor-acceptor (D-A) that exhibit TADF. In addition, four EL properties, EQE, power efficiency (PE), CIE<sub>xy</sub>

\*Authors to whom correspondence should be addressed.

coordinates, and normalized EL emissions, are presented to compare the two emitters.

## 2. EXPERIMENTAL DETAILS

### 2.1. Structural Design by DFT Calculation

In DPS, an oxygen unit has strong electronegativity, which results in the electron-withdrawing nature of the sulfonyl group. The sulfonyl group of DPS exhibits a tetrahedral geometry, which limits the conjugation of compounds. Consequently, DPS is the best-known typical electron acceptor component in TADF molecules.<sup>16</sup> The derivative compounds based on DPS are expected to show a large twisted conformation between the phenyl ring and the acridine units by leading to a comparatively small  $\Delta E_{ST}$  and the effective separation of molecular orbitals. However, many TADF materials cannot achieve a deep-blue emission and show rather broad EL spectra. Therefore, in this study, **D1-DPS** and **D2-DPS** that consisting of a common acceptor group with two different spiro-acridine units were designed and calculated.

We investigated the factors responsible for the absorption energy and the electron population of molecular orbitals by performing DFT and time-dependent density functional theory (TD-DFT) calculations in the ground state by using the dependence on the amount of charge transfer (CT) from the donor to acceptor for the optimal HF percentage in the TD-DFT exchange-correlation. The geometries in the gas phase were optimized by applying the DFT method and using the B3LYP exchange-correlation function with the 6-31G\* basis set in the Gaussian 09 program package. We determined an optimal HF% (OHF) by using the Multiwfn program to analyze the optimal orbital composition for obtaining a CT amount ( $q$ ) from the donor to the acceptor; the optimal HF% was proportional to the CT amount according to the formula  $\text{OHF} = 42q$ . According to the Franck-Condon principle, the crossing point between absorption and emission corresponds to the  $E_{00}$  of the CT transitions, as  $E_{VA}(S_1) - E_{00}(S_1) = E_{00}(S_1) - E_{VE}(S_1)$ . The value of  $E_{00}(S_1)$  was calculated as  $(E_{VA}(S_1, \text{OHF}) + E_{VE}(S_1, \text{OHF}))/2$ .

The electron distributions of the highest occupied molecular orbital (HOMO) and the lowest unoccupied molecular orbital (LUMO) in these materials were calculated using the DFT method with the optimized ground-state molecular geometry, as shown in Figure 1.

The HOMO distribution was localized on the acridan moieties, whereas the LUMO was localized on the DPS moiety. The dihedral angles of **D1-DPS** and **D2-DPS** were almost perpendicular. These larger dihedral angles led to the separation between the HOMO and the LUMO, which resulted in a small  $\Delta E_{ST}$ .

Table I shows the calculated CT amount ( $q$ ), OHF%, dihedral angle,  $S_1$  and  $T_1$  state energies,  $\Delta E_{ST}$ , and emission wavelengths [ $E_{VE}(S_1)$ ] of **D1-DPS** and **D2-DPS**.

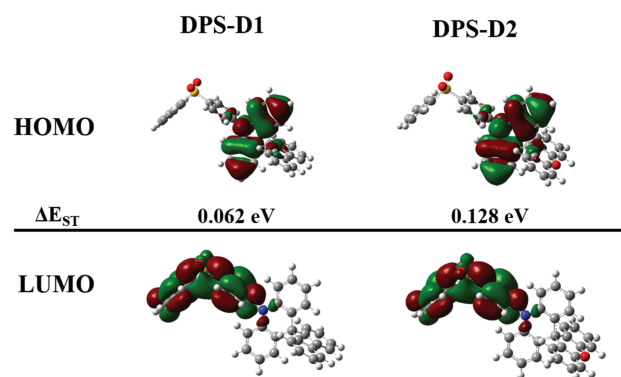


**Figure 1.** Optimized geometries and calculated HOMO and LUMO density maps for **D1-DPS** and **D2-DPS**.

These molecules showed sufficiently small  $\Delta E_{ST}$  between the  $S_1$  and  $T_1$  of **D1-DPS** (0.062 eV) and **D2-DPS** (0.128 eV). These small values indicate that the energy barrier is sufficient for reverse intersystem crossing (RISC) to exhibit TADF characteristics.

### 2.2. Synthesis

#### 2.2.1. General

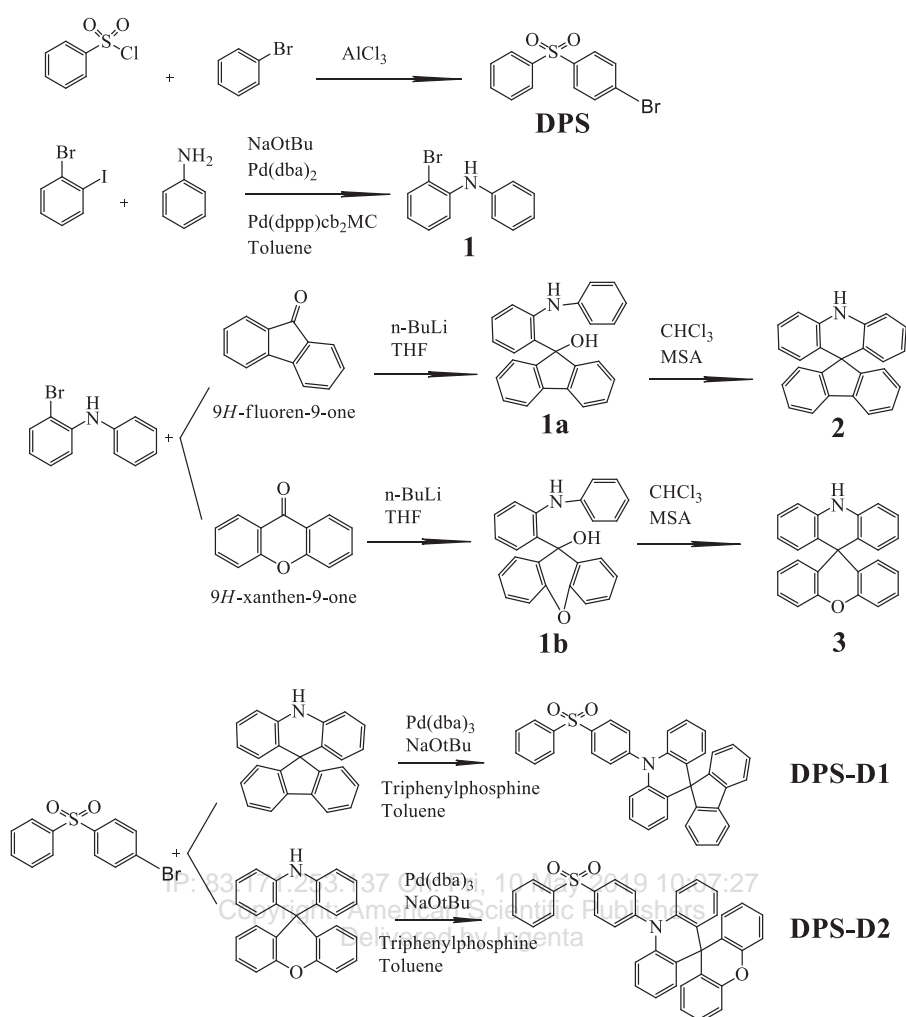
Most reactants and solvents were purchased from commercial sources and used without further purification. Tetrahydrofuran (THF) was purified using a solvent purification system (Korea Kiyon Co., Ltd.). <sup>1</sup>H-NMR was recorded using a Bruker DRX400 spectrometer in DMSO or CDCl<sub>3</sub>. UV-Vis spectra were obtained by a UV-Visible spectroscopy (Agilent 8453). PL spectra were recorded using a fluorescence spectrometer (LS55, PerkinElmer precisely) with hexane, dichloromethane (MC or DCM), toluene, and dimethylformamide (DMF) as solvents to investigate the solvent polarity in solution PL spectra. All the reaction synthesis processes are described in Scheme 1.

#### 2.2.2. Synthesis of 1-Bromo-4-(phenylsulfonyl)Benzene (DPS)<sup>10</sup>

Benzenesulfonyl chloride (5 g, 28 mmol) and bromobenzene (4.84 g, 30.8 mmol) were placed in a round bottom flask with N<sub>2</sub> charging. Anhydrous aluminum chloride

**Table I.** Calculated CT amount ( $q$ ), OHF%,  $S_1$  and  $T_1$  state energies,  $\Delta E_{ST}$ , and emission wavelengths [ $E_{VE}(S_1)$ ] of **D1-DPS** and **D2-DPS**.

Parameter	D1-DPS	D2-DPS
CT amount ( $q$ )	0.879	0.877
Optimal HF%	0.369	0.368
$E_{0-0}(S_1)$	3.129	3.161
$E_{0-0}(T_1)$	3.067	3.033
$\Delta E_{ST}$	0.062	0.128
$E_{VE}(S_1)$ (nm)	429.2	424.5
HOMO	-5.130	-5.200
LUMO	-1.607	1.637
Dihedral angle	89.9°	89.9°
Oscillator strength ( $f$ )	0.000	0.000



**Scheme 1.** Reaction scheme for **D1-DPS** and **D2-DPS**.

(3.73 g, 28 mmol) was dissolved in a small amount of upper reactant and added slowly to the flask with continuous stirring. The mixture first changed to red and then to dark reddish brown. The mixture was refluxed at 90 °C for 7–8 h. The progress of the reaction was monitored by thin layer chromatography (TLC) with a mixture of hexane and ethyl acetate (5:1). After the reaction was completed, the mixture was cooled and poured into a mixture of deionized water and concentrated HCl. The obtained product was recrystallized by ethanol.

*Yield:* 74.4%;  $^1\text{H-NMR}$  (500 MHz,  $\text{CDCl}_3$ ):  $\delta$  (ppm) 7.84–7.82 (*d*, 2H), 7.75 (*d*, 2H), 7.72–7.68 (*d*, 2H), 7.60–7.58 (*d*, 2H), 7.54–7.50 (*t*, 1H), 7.46–7.42 (*t*, 2H).

### 2.2.3. Synthesis of 2-Bromo-N-Phenylaniline (**1**)<sup>15</sup>

Intermediate compound **1** was synthesized by a Buchwald-Hartwig reaction. 1-bromo-2-iodobenzene (10 g, 35.3 mmol), sodium-*tert*-butoxide (*t*-BuONa, 4.76 g,

49.4 mmol), bis(dibenzylideneacetone)palladium(0) ( $\text{Pd}(\text{dba})_2$ , 0.2 g, 0.35 mmol), and [1,1-bis(diphenylphosphino)ferrocene]dichloropalladium ( $\text{Pd}(\text{dppp})\text{Cl}_2$ , 0.52 g, 0.71 mmol) were placed and stirred in a round bottom flask with  $\text{N}_2$  charging. Then aniline (3.23 g, 35.3 mmol) and 20 ml of toluene were injected. The mixture was refluxed at 115 °C for 2 h. The reaction was monitored by TLC with a mixture of hexane and ethyl acetate (10:1). After the reaction was completed, the mixture was quenched by a saturated NaOH solution and then worked up using water and ethyl acetate. The extracted organic layer was dried by anhydrous  $\text{MgSO}_4$ . It was then filtered by celite and purified by column chromatography with hexane and ethyl acetate. A slightly yellow oil was obtained.

*Yield:* 55.5%;  $^1\text{H-NMR}$  (500 MHz,  $\text{CDCl}_3$ ):  $\delta$  (ppm) 7.51–7.48 (*d*, 2H), 7.32–7.28 (*t*, 2H), 7.24–7.22 (*d*, 1H), 7.14–7.12 (*d*, 3H), 7.04–7.00 (*t*, 1H), 6.73–6.69 (*t*, 1H), 6.07 (*s*, 1H).

#### 2.2.4. Synthesis of 10-(4-(phenylsulfonyl)phenyl)-10H-Spiro[acridine-9,9'-fluorene] (D1-DPS)<sup>8,11</sup>

To obtain the **D1-DPS**, compound **1a** of the –OH formation reaction, and compound **2** of the cyclization reaction were synthesized. Compound **1** (3 g, 12 mmol) was dissolved in 50 ml of anhydrous tetrahydrofuran (THF) under high purity argon in a one neck round bottom flask. It was cooled to –78 °C using solid carbon with acetone and then *n*-butyllithium (2.5 M in cyclohexane, 24.7 mmol) was added dropwise slowly. Stirring was continued for 1 h before, cooling for 20–30 min. Then a solution of 9-fluorenone (2.4 g, 13.3 mmol) in THF was added at –78 °C under an argon atmosphere. The mixture was stirred for 3 h in the same environment. The reaction was completed after the confirmation of compound **1a**. Two side products and reactants appeared by TLC with a solution of hexane and ethyl acetate (10:1). Additional quenching was not required. The mixture was then worked up using water and dichloromethane. The extracted organic layer was dried by anhydrous MgSO<sub>4</sub>.

For compound **2**, compound **1a** was placed in a one-neck round bottom flask, to which, chloroform (10 ml) and methane sulfonic acid (MSA, 5 ml) were added while stirring at room temperature for 15 min. The progress of the reaction was monitored by TLC with a solution of hexane and ethyl acetate (5:1). The resulting mixture was quenched by saturated aqueous NaHCO<sub>3</sub> and extracted with dichloromethane after the reaction completed. The solid product was recrystallized using chloroform and hexane. A slightly yellow solid product was obtained, which was then purified by column chromatography with hexane and ethyl acetate.

Two intermediates, the **DPS** acceptor and the compound **2** donor, were reacted for **D1-DPS** by the Buchwald-Hartwig amination. Compound **2** (0.5 g, 1.38 mmol), **DPS** (0.48 g, 1.38 mmol), Pd(dba)<sub>2</sub> (0.008 g, 0.014 mmol), *t*-BuONa (0.27 g, 2.77 mmol), and triphenylphosphine (0.003 g, 0.011 mmol) showed high purity Ar charging. Then toluene (20 ml) was added and refluxed for 5 h at 115 °C. Quenching was not required. The resulting mixture was worked up using ethyl acetate and water. A small amount of water in the extracted organic layer was removed by MgSO<sub>4</sub> and filtered with celite to remove the inorganic materials. Finally, column chromatography was applied with hexane and dichloromethane. The white solid product was recrystallized by hexane.

Yield: 59.9%; <sup>1</sup>H-NMR (500 MHz, CDCl<sub>3</sub>): δ (ppm) 8.30–8.28 (*d*, 2H), 8.11–8.10 (*d*, 2H), 7.81–7.79 (*d*, 2H), 7.64–7.61 (*t*, 4H), 7.39–7.36 (*t*, 4H), 7.26–7.14 (*d*, 4H), 7.10–7.08 (*d*, 2H), 6.91–6.85 (*t*, 2H), 6.60–6.56 (*t*, 2H), 6.41–6.36 (*d*, 2H), 6.26–6.20 (*d*, 2H). Elem. Anal. found for C<sub>37</sub>H<sub>25</sub>NO<sub>2</sub>S: C, 75.1773; H, 4.5610; N, 2.1293; O, 9.3124; S, 5.0175.

#### 2.2.5. Synthesis of 10-(4-(phenylsulfonyl)phenyl)-10H-Spiro[acridine-9,9'-xanthene] (D2-DPS)<sup>8,11</sup>

The other dopant material, **D2-DPS**, was synthesized by the same procedure as described for **D1-DPS** in Section 2.2.4. Only the reactant was changed in each step. First, the –OH formation reaction to obtain the compound **1b** and the cyclization reaction for compound **3** were performed sequentially. Compound **1** (3 g, 12 mmol) was dissolved in 50 ml of anhydrous THF under high purity argon. In the *n*-butyllithium reaction, a solution of xanthone (2.61 g, 13.3 mmol) in THF was used. The reaction was ended after the confirmation of compound **1b** by TLC with a solution of hexane and ethyl acetate (10:1). Additional quenching was not required. The mixture was then worked up using water and dichloromethane. The extracted organic layer was dried by anhydrous MgSO<sub>4</sub>.

For compound **3**, compound **1b** was placed in one-neck round bottom flask, to which chloroform (10 ml) and methane sulfonic acid (MSA, 5 ml) were added with stirring at room temperature for 15 min. The progress of the reaction was monitored by TLC with a solution of hexane and ethyl acetate (5:1). The resulting mixture was quenched with saturated aqueous NaHCO<sub>3</sub> and extracted with dichloromethane after the reaction was completed. In addition, the solid product was recrystallized using chloroform and hexane. The obtained slightly yellow solid product was purified by column chromatography with hexane and ethyl acetate. A solid white product was obtained.

Two intermediates, **DPS** acceptor and compound **3**, were reacted for **D2-DPS** using Buchwald-Hartwig amination with the same procedure describe in Section 2.2.4. A solid white product was obtained.

Yield: 44.5%; <sup>1</sup>H-NMR (500 MHz, CDCl<sub>3</sub>): δ (ppm) 8.28–8.26 (*d*, 2H), 8.11–8.09 (*d*, 2H), 7.70–7.67 (*t*, 2H), 7.64–7.61 (*t*, 4H), 7.26–7.14 (*d*, 4H), 7.10–7.08 (*d*, 2H), 6.96–6.94 (*t*, 2H), 6.87–6.84 (*t*, 4H), 6.71–6.68 (*t*, 2H), 6.15–6.12 (*d*, 2H). Elem. Anal. found for C<sub>37</sub>H<sub>25</sub>NO<sub>3</sub>S: C, 78.7617; H, 4.5699; N, 2.3221; O, 8.6813; S, 5.5692.

#### 2.3. Device Fabrication and Measurement

We fixed the emitter concentration to a 10 wt% with the ADN host material in the EML layer. The device was fabricated by the deposition of the following materials and layers: indium-in-oxide (ITO) (150 nm)/TCTA (50 nm)/10 wt% emitter: ADN (20 nm)/TPBi (30 nm)/LiQ (2 nm)/Al (100 nm). **D1-DPS** and **D2-DPS** emitters were used separately, as shown in Figure 2. In this work, ITO substrates with a sheet resistance of 10 Ω/sq were used, and they were treated with oxygen plasma at 2 × 10<sup>–5</sup> Torr at 125 W for 2 min. The organic layers were deposited by thermal evaporation through a shadow mask under a high vacuum (8 × 10<sup>–5</sup> Torr) condition. A water-getter was used to absorb the residue moisture in the encapsulated device. To measure the EL properties, Keithley SMU 238 and Minolta CS-100A were used, and 4 mm<sup>2</sup> of OLEDs

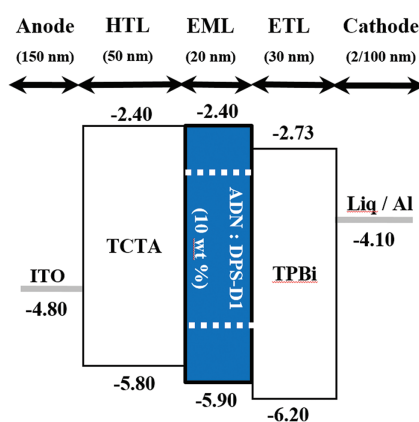


**Figure 2.** Device structure using **D1-DPS** (Device 1). In **D2-DPS** (Device 2), all components were exactly the same as in device 1, including the doping concentration.

area were examined. The EL spectra and CIE coordinates were identified and measured by a Minolta CS-2000 spectroradiometer. All measurements were carried out at room temperature under ambient conditions.

### 3. RESULTS AND DISCUSSION

#### 3.1. Material Property

We investigated the photochemical and photophysical properties of two materials. As shown in Figure 3, UV-Vis absorption and PL spectra were described using both solution of **D1-DPS** and **D2-DPS** in MC. These molecules showed three absorption peaks at about 250 nm, 275 nm, and 360 nm, respectively in UV-Vis spectra. The peak at 360 nm appeared by charge transfer (CT) property. In the solution PL spectra at room temperature, **D2-DPS**, which introduced an oxygen atom into the acridine donor unit, showed 5 nm of blue shift compared with **D1-DPS**. The excitation wavelength was fixed at 275 nm for both molecules during the PL measurements. Each material

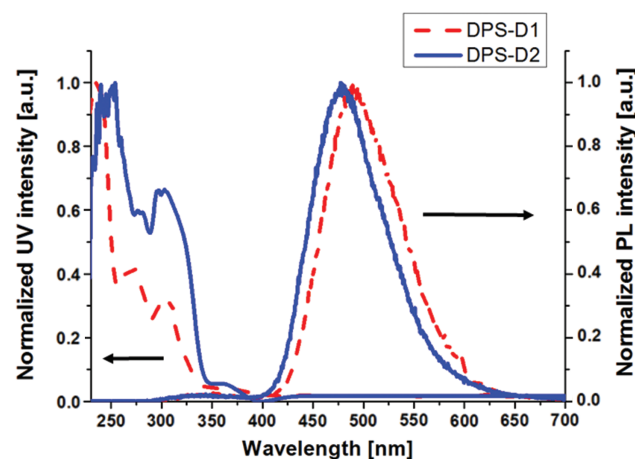


**Figure 3.** UV/PL spectra of **D1-DPS** and **D2-DPS** dissolved in MC that has a cut off wavelength of 233 nm. Each solution was optimized at  $10^{-5}$  M.

showed deep-blue emission at 470~480 nm. The result indicates that two final products functioned as emitters better than the host did. They were doped in the well-known host material in each device. The emission peak of the host and the absorption of the emitter should overlap to produce an effective energy transfer from the host to the dopant material in the EML. These materials overlapped lightly in the range of 350–400 nm.

We also confirmed polarity dependence using the Lippert-Mataga calculation, which indicated TADF characteristics. The excited state of an emitter is stabilized in more polar solvents, which is expected in an ICT property. In this phenomenon, the excited electrons were moved from the donor group to acceptor, and then the singlet was formed the triplet by ICT.

The negative slope in the Lippert-Mataga plot showed the solvatochromism of emitters according to the polarity of the solvents, and the emission characteristics were confirmed by ICT. PL fluorescence emission peaks were measured in four different solvents, hexane, toluene, MC, and DMF. The emission peaked in DMF at about 490 nm, which means a small amount of red shift was obtained because of its molecular structures. Since chemical structures of **D1-DPS** and **D2-DPS** restrict the rotational, bending, and stretching modes because of their spiral structure. These chemical structures interrupted the Frank-Condon factor of the acridine moiety and led to the blue shift in the PL emission wavelength.<sup>4</sup> This result indicates that the electron donor group did not affect the molecule orbitals.

As shown in Figure 4, **D2-DPS** demonstrated a stronger emission intensity and a larger negative slope than **D1-DPS** did. **D2-DPS** was expected to procedure more deep-blue EL emissions than **D1-DPS**.

As shown in Figure 5, mass transitions of the two emitters were measured to investigate their thermal stability. The emitters showed a similar tendency: 10% loss of mass

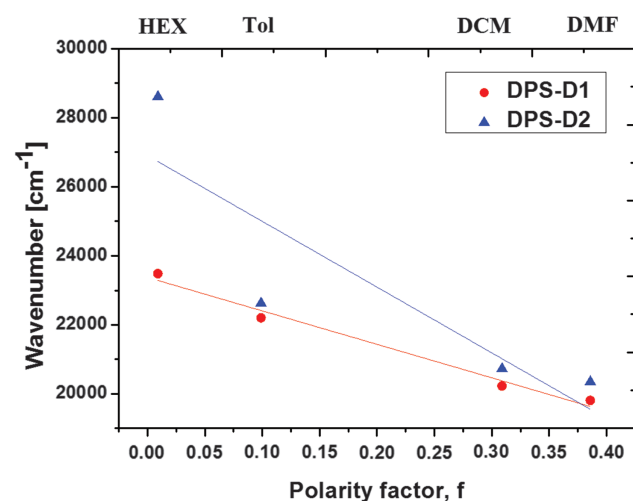


**Figure 4.** Lippert-Mataga plot using four different solvents (hexane, toluene, MC, and DMF) of **D1-DPS** and **D2-DPS**.

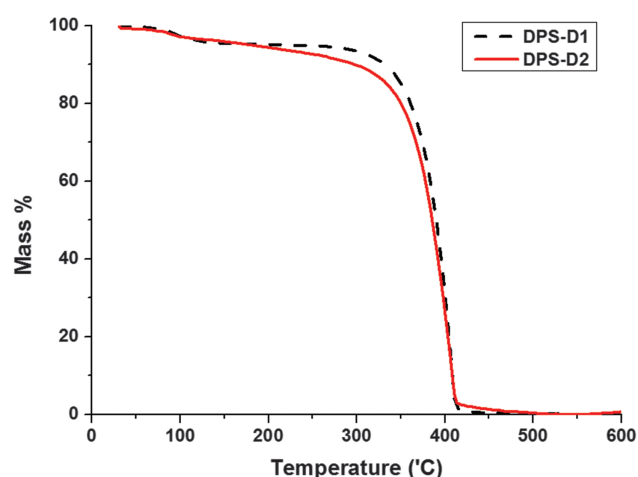


**Figure 5.** TGA curve showing mass transitions of **D1-DPS** and **D2-DPS** in  $N_2$  atmosphere.

until 325 °C. In the next step from 325 °C to 410 °C, the emitters began to lose weight, which indicated that decomposition also began at 410 °C. Hence, both emitters were thermally stable until 410 °C. This stability resulted from the twist structure that was designed to represent the TADF property.

### 3.2. Device Performance

The normalized EL spectra of blue OLEDs at 9 V are shown in Figure 6(a). Device 1 and Device 2 showed

similar electro-emission peaks at 441 nm and 436 nm, respectively. In the Figure 6(d), the  $CIE_{xy}$  coordinates show that the emission of the fabricated devices was in the deep-blue region, which means good color purity. The CIE coordinates (0.153, 0.064) in Device 1 and (0.152, 0.065) in Device 2 were observed. **D1-DPS** and **D2-DPS** exhibited the maximum external EL quantum efficiencies (EQE) of 4.13% and 5.05%, respectively, as shown in Figure 6(b). Both devices achieved slight efficiency roll-off characteristics, so the decay time of the TADF mechanism was expected to be brief. These results could have been caused by discordance between the absorption peak of the two emitters at 360 nm and the emission peak of the ADN at 400 nm. This discordance could have led to the lower energy transfer between the luminescence materials. Figure 6(c) shows the luminescence-PE spectra. Device 2 could not endure more than 1,300  $cd/m^2$  of high luminescence. Device 2 showed a lower PE than Device 1. In addition, the  $J$  (current density)– $V$  (voltage) graph was measured. Device 1 and Device 2 achieved 800  $mA/cm^2$  and 85  $mA/cm^2$  at 9 V, respectively. Because of their structural similarity, **D1-DPS** and **D2-DPS** showed similar performance. However, **D2-DPS** demonstrated only one-third of the luminescence that **D1-DPS** demonstrated. Thus, **D2-DPS** functioned better than **D1-DPS** did in luminescence efficiency. Fluorescent devices generally use low doping concentration (1~5 wt%) to obstruct the triplet–triplet annihilation (TTA) by suppressing the Dexter energy

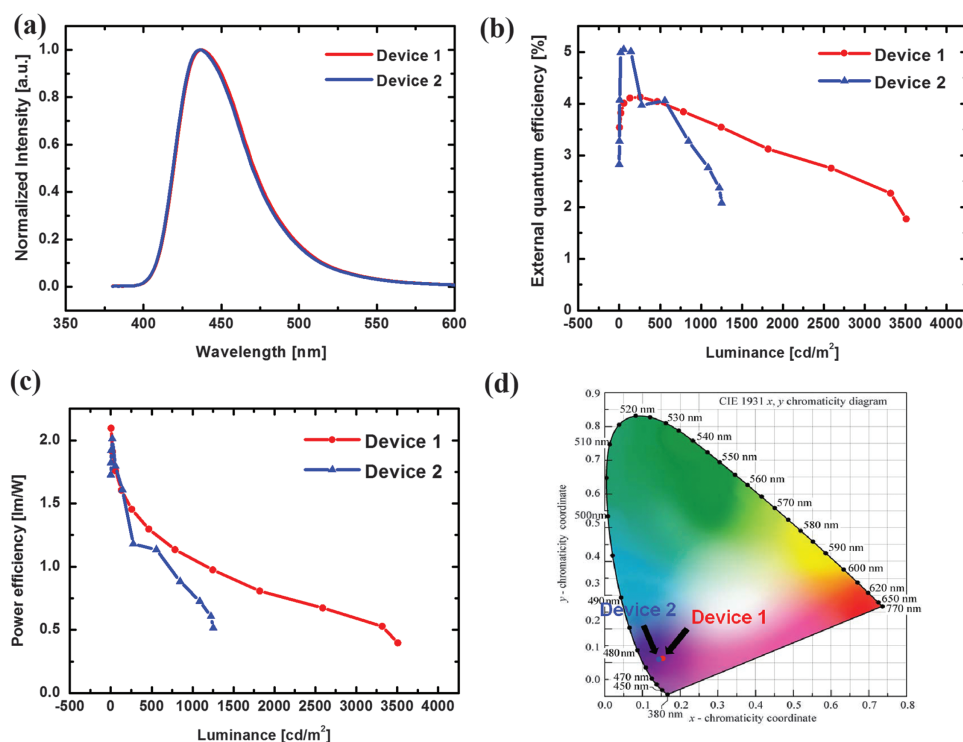


**Figure 6.** Performance of Device 1 (**D1-DPS**) and Device 2 (**D2-DPS**). (a) Normalized EL characteristics, (b) luminescence-EQE characteristics, (c) luminescence-PE, and (d)  $CIE_{xy}$  coordinates characteristics of blue OLEDs.

transfer (DET). However, these two emitters inhibited concentration quenching at a concentration of 10 wt%.<sup>18</sup> Concentration quenching was suppressed in the devices using **D1-DPS** and **D2-DPS** emitters because the bulky and largely twisted characteristics of the emitter molecules obstruct  $\pi$ -stacking between them. Thus, these molecules are promising host-free TADF deep-blue emitters because they inhibit concentration quenching.

#### 4. CONCLUSION

In summary, we observed deep-blue OLEDs that exhibited TADF characteristics, which we confirmed through photochemical analysis by designing and synthesizing two DPS derivative emitters, **D1-DPS** and **D2-DPS**. The  $\Delta E_{ST}$  values of **D1-DPS** and **D2-DPS** were small enough to demonstrate the TADF phenomenon through a small spatial overlap between the HOMO and the LUMO; there was a large dihedral angle between the donor and the acceptor. Device 1 and Device 2, which were doped with 10 wt% of **D1-DPS** and **D2-DPS**, exhibited the maximum EQE of 4.13% and 5.05%, respectively, with deep-blue emissions having the CIE coordinates of (0.153, 0.064) and (0.152, 0.065), respectively. Concentration quenching was suppressed in the devices using **D1-DPS** and **D2-DPS** emitters. These results showed that these molecules are candidate materials for host-free TADF deep-blue emitters.

**Acknowledgments:** This work was supported by the Basic Science Research Program through the National Research Foundation of Korea (NRF) and, funded

by the Ministry of Education (Nos. 201502080003, 2017R1D1A1B03028107 and 2015R1A6A1A03031833).

#### References and Notes

1. X. Wei, Y. Chen, R. Duan, J. Liu, R. Wang, Y. Liu, Z. Li, Y. Yi, Y. Yamada-Takamura, P. Wang, and Y. Wang, *J. Mater. Chem. C* 5, 12077 (2017).
2. Q. Zhang, B. Li, S. Huang, H. Nomura, H. Tanaka, and C. Adachi, *Nature Photonics* 8, 326 (2014).
3. B. Huang, Q. Qi, W. Jiang, J. Tang, Y. Liu, W. Fan, Z. Yin, F. Shi, X. Ban, H. Xu, and Y. Sun, *Dyes and Pigments* 111, 135 (2014).
4. M. Numata, T. Yasuda, and C. Adachi, *Chem. Commun.* 51, 9443 (2015).
5. H. Wang, L. Xie, Q. Peng, L. Meng, Y. Wang, Y. Yi, and P. Wang, *Adv. Mater.* 26, 5198 (2014).
6. G. Mehes, H. Nomura, Q. Zhang, T. Nakagawa, and C. Adachi, *Angew. Chem. Int. Ed.* 51, 11311 (2012).
7. S. Huang, Q. Zhang, T. Nakagawa, K. Kuwabara, K. Yoshizawa, and C. Adachi, *J. Chem. Theory Comput.* 9, 3872 (2013).
8. S. O. Jeon and J. Y. Lee, *Tetrahedron* 66, 7295 (2010).
9. G. H. Lee, D. Y. Kwon, and Y. S. Kim, *Mol. Cryst. Liq. Cryst.* 621, 1 (2015).
10. A. Wani and S. Mahajan, *Am. J. PharmTech. Res.* 4, 1057 (2014).
11. A. H. Parham, P. Stoessel, T. Eberle, A. Jatsch, J. V. Kroeber, T. Grossmann, and C. Plumm, US patent US20170141327A1 (2014).
12. G. H. Lee and Y. S. Kim, *Polym. Bull.* 73, 2439 (2016).
13. F. Zinna, U. Giovanella, and L. D. Bari, *Adv. Mater.* 27, 1791 (2015).
14. Z. Yang, Z. Mao, Z. Xie, Y. Zhang, S. Liu, J. Zhao, J. Zhao, J. Xiu, Z. Chi, and M. P. Aldred, *Chem. Soc. Rev.* 46, 915 (2017).
15. B. H. Yang and S. L. Buchwald, *J. Organometallic Chem.* 576, 125 (1999).
16. M. Liu, Y. Seino, D. Chen, S. Inomata, S. J. Su, H. Sasabe, and J. Kido, *Chem. Soc. Rev.* 51, 16353 (2015).
17. K. Wang, C. J. Zheng, W. Liu, K. Liang, Y. Z. Shi, S. L. Tao, C. S. Lee, X. M. Ou, and X. H. Zhang, *Adv. Mater.* 29, 1701476 (2017).
18. J. Y. Lee, N. Aizawa, M. Numata, C. Adachi, and T. Yasuda, *Adv. Mater.* 29, 1604856 (2017).

Received: 23 June 2018. Accepted: 28 October 2018.